Spatial resolution and temperature matter for mapping Cerrado wetlands and dry grasslands

Paulo N. Bernardino[1,2,*], Larissa Verona[1], Natashi Pilon[2], Christophe Metsu[3,4], Rafael S. Oliveira[2], Ben Somers[3,4], Koenraad Van Meerbeek[3,4], Amy E. Zanne[1]

[1] Cary Institute of Ecosystem Studies, 2801 Sharon Turnpike, Millbrook NY 12545, United States.

[2] Department of Plant Biology, University of Campinas, Rua Monteiro Lobato 255, Campinas SP 13083-970, Brazil.

[3] Division Forest, Nature and Landscape, KU Leuven, Celestijnenlaan 200E, Leuven 3001, Belgium.

[4] KU Leuven Plant Institute (LPI), Kasteelpark Arenberg 31, Leuven 3001, Belgium.

* Corresponding author: paulo.nbernardino@gmail.com; +55 19 996450886

ABSTRACT

Wetlands in the Brazilian Cerrado play key roles in regional carbon and water cycles but remain poorly mapped due to their patchy distribution and seasonal variability. Therefore, knowing where and when they occur is urgently needed. To address this gap, we evaluated how spatial resolution and inclusion of thermal (on top of traditional multispectral) data affected wetland vs. dry grassland mapping accuracy using Unoccupied Aerial Vehicle (UAV) imagery. Additionally, we investigated variable importance and how including topography and vegetation patch size as post-processing constraints improved accuracy. We used multispectral and thermal data with resolutions ranging from 0.10 to 1.50 m to train and validate Random Forest models across two seasons. Mapping accuracy increased with pixel size up to 1.0 m, declining at coarser resolutions. Incorporating land surface temperature (LST) significantly improved classification, increasing accuracy by 4.2 to 7.3 percentage points depending on the season. Grassland type classification was primarily driven by the Normalized Difference Vegetation Index (NDVI) and LST, with the latter being especially discriminant in the wet season. Accuracy was further improved by incorporating ancillary data, reaching up to 94% in the wet season. When compared with state-of-the-art land cover maps for Brazil, our drone-based results reveal a wetland extent more than four times larger in the study area than previously reported, underscoring the widespread underestimation of these ecosystems. These findings highlight the value of combining UAV-based multispectral and thermal data for identifying and monitoring Cerrado wetlands, providing essential information to guide conservation efforts in this threatened ecosystem.

Keywords: Cerrado, drone, grasslands, multispectral, thermal, wetlands.

1. INTRODUCTION

The Brazilian Cerrado is a global biodiversity hotspot, home to approximately 4,400 endemic plants and 117 endemic vertebrate species (Myers et al., 2000), and estimated to store 2 Tg C/ha/year (Sawyer, 2009). Cerrado wetlands, in particular, regulate hydrological flows by storing rainfall and sustaining perennial rivers (Bassani et al., 2025; Durigan et al., 2022), and in some regions, these wetlands can store ~ 1,500 Mg C/ha (Verona et al., 2026). Despite their ecological importance, large-scale agricultural expansion threatens carbon stocks and water provision across wetlands in the Cerrado (Ribeiro et al., 2011). Moreover, these wetlands remain poorly characterized, and their extent is likely underestimated due to mapping limitations. Wetlands in the Brazilian Cerrado occur as scattered patches across a heterogeneous landscape, often only m to a few km in extent and bordering savannas, dry grasslands (which are never waterlogged), and riparian forests. This fine-scale spatial variability makes them particularly difficult to map using widely available satellite products. Errors of only tens of m can translate into substantial under- or over-estimation of wetland extent. Moreover, current national land cover products (MapBiomas, 2024a) often miss seasonal expansions, since for mapping the Cerrado region, they rely on imagery from periods when wetlands are contracted (i.e., the dry season; MapBiomas, 2024b). As such, these products primarily represent permanently flooded systems, leading to a substantial underestimation of Cerrado wetland extent. As a result, we still lack accurate, spatially explicit knowledge of where Cerrado wetlands occur and how they vary through time, representing a major obstacle for quantification of their contributions to water and carbon cycles and their protection and conservation.

Unoccupied Aerial Vehicles (UAVs), or drones, offer an alternative for capturing the fine spatial and temporal patterns of Cerrado wetlands by providing cm to m scale imagery across seasons. However, a fundamental challenge when using drones to map vegetation types involves finding the optimal spatial resolution for the classification goal (Liu et al., 2020; Woodcock and Strahler, 1987). Too fine resolutions can result in a higher intra- than inter-class spectral variability, leading to spectral confusion and hampering class separability (Liu et al., 2020; Meddens et al., 2011). Therefore, a better understanding of the relationship between spatial scale and mapping accuracy in Cerrado wetlands is needed not only to determine the strengths and limitations of using drone imagery for monitoring wetlands (Steenvoorden and Limpens, 2023) but also to explore potential ways to improve satellite-based large-scale mapping of these important and understudied vegetation types.

Further, vegetation similarity between dry and waterlogged grasslands can hamper classification using only RGB or multispectral data. Although subtle differences exist, they might be easier (or only) captured through the use of hyperspectral data (Adam et al., 2010; Jarocińska et al., 2023). An alternative to costly hyperspectral sensors could be using other system characteristics that differentiate these vegetation types, such as surface temperature differences. Wetlands often exhibit distinct thermal regimes compared to adjacent land cover types (Hemes et al., 2018; Muro et al., 2018), largely due to differences in soil moisture and evapotranspiration (Hemes et al., 2018; Oke, 1987; Wu et al., 2021). Such thermal contrasts, detectable by drone-mounted thermal sensors, may therefore enhance discrimination between vegetation types and improve mapping accuracy.

Here, we explore how spatial resolution, thermal remotely-sensed data, and ancillary environmental data influence the accuracy of UAV-based mapping of Cerrado wetlands. Additionally, we assessed how different predictor variables affect wetland classification in distinct seasons. We hypothesize that mapping accuracy will be highest when spatial resolution matches the scale of the classification target (i.e., plant communities), therefore, in the scale of m, and not cm or tens of m. We further hypothesize that adding thermal data will facilitate discrimination between wet and dry grasslands, improving mapping accuracy. Finally, we hypothesize that using ancillary data on topography and vegetation community patch sizes will further improve classification accuracy. Specifically, we address four questions: (1) What is the optimal spatial resolution for mapping Cerrado wetlands using UAV data? (2) How does the inclusion of thermal data affect mapping accuracy? (3) Which variables contribute most to classification performance? (4) Does incorporating ancillary environmental data, such as terrain topography, further improve wetland mapping?

2. METHODS

2.1. Study site

Our study site was located in the Cerrado in Chapada dos Veadeiros National Park (CVNP), Goiás, Brazil (Fig. 1). There is a mosaic of different vegetation types in the park, ranging from open ecosystems dominated by grasslands to closed ecosystems, including woody savannas and riparian forests (Lewis et al., 2022; Ribeiro and Walter, 2008). For this study, we selected a ~0.5 km^2 gradient from ever-wet peatland (continuously waterlogged grassland) to seasonal wetland (seasonally waterlogged) to dry grassland (never waterlogged).

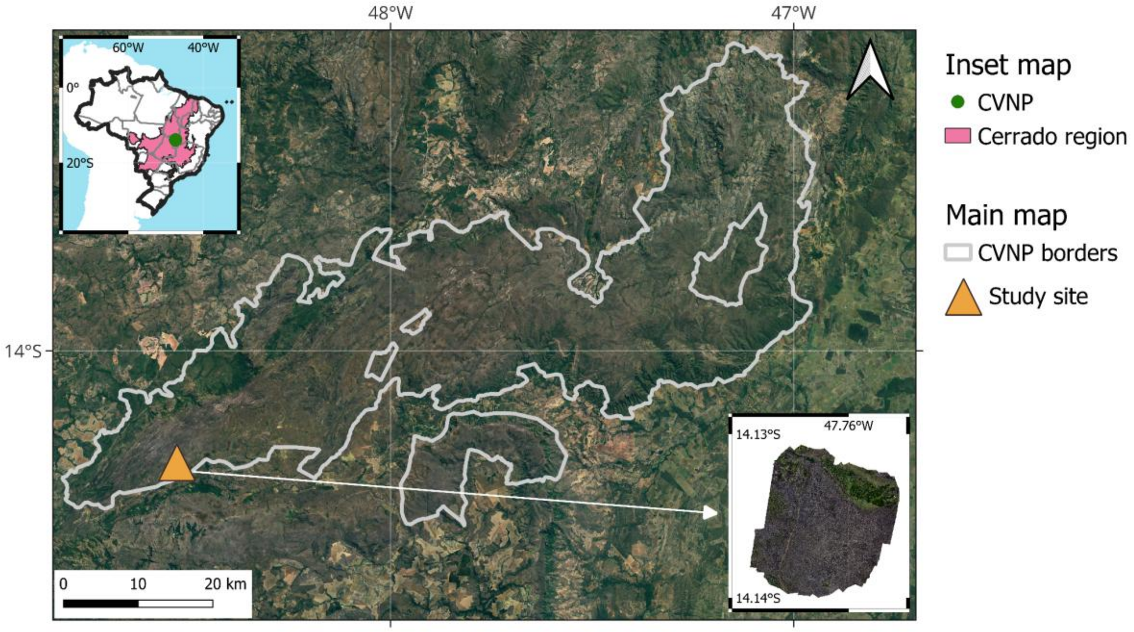

Fig. 1. Map of the study site. The *Chapada dos Veadeiros* National Park (CVNP) borders are shown in gray with a true-color satellite image (Google Earth, 2018) in the background. The study site location is represented as an orange triangle. The top left inset map shows the location of CVNP in Brazil, as a green dot, and the Cerrado region in pink. The bottom right inset map shows a true-color drone image from the study site in the transition season (December 2024).

The mean annual precipitation in the park is ~1,365 mm/year, with a marked dry season between June and August and a wet season between December and February (Funk et al., 2015). We carried out two field campaigns including, (1) the transition from the dry to wet season (December 2024) and (2) the peak of the wet season (February 2025). This sampling allows us to test for potential seasonal differences.

2.2. Drone flights and reference data

To map the extent of the wetlands, we flew a DJI Mavic 3 Multispectral and a DJI Mavic 3 Thermal drone over the study site during each field campaign. The flights were performed between 10:00 am and 2:00 pm to avoid tree shading as much as possible (Maes, 2025). Flights were planned using QGIS version 3.28.12 to create a polygon covering the full study area, which was then exported and loaded to the drones' remote controllers. The flight area was approximately 0.45 km^2 in the transition season, and we expanded it to 0.54 km^2 in the peak of the wet season to guarantee that the flight area would cover the border between the waterlogged and dry grassland. Based on the polygon generated in QGIS, the flight mission was planned on DJI's remote controller app using the following settings: single grid, nadir orientation, 100 m flight altitude, 75% frontal overlap, 80% side overlap, 5 m/s flight speed (Maes, 2025). The same flight mission planning was used for the multispectral and thermal drones. After drone imagery pre-processing (section 2.3), the resulting orthomosaic raster files had a spatial resolution of ~1.3 cm for the multispectral imagery and 3.8 cm for the thermal imagery.

To have in situ reference information, we sampled reference points (i.e., waterlogged and dry grassland locations) in the field using a Garmin GPSMAP 65s with 1.5 m accuracy, during field campaigns. These reference points were used to train and validate a supervised classification machine learning model (i.e., Random Forest (RF); section 2.4), to classify the studied area into one of three classes: waterlogged grassland, dry grassland, and "other", which included all other land cover types present in the study area (i.e., bare soil, water bodies, large trees). We sampled 60 points for waterlogged grasslands and 60 points for dry grasslands. The points were collected in areas with homogeneous cover, i.e., not too close to other land cover types. These selections were made visually in the field, with an estimated distance of at least 5 m. The number of sampled reference points represents a trade-off between sample size and feasibility: sampling enough points to train and validate the RF model, and what is feasible during a field campaign. For the "other" class, we created 60 polygons in QGIS using a visual interpretation of the true color images obtained from the multispectral drone. Such polygon creation is possible for this class, but not for the grassland classes, since bare soil, water bodies, and trees are easily distinguishable in the images, while a precise differentiation between waterlogged and dry grasslands is only possible in situ. Next, we made 5 m buffers around the sampled grassland points, resulting in 10 x 10 m square polygons surrounding the points. All pixels within these polygons were considered to be from the same class as the sampled point, and thus, used to train or validate the RF models.

2.3. Drone imagery pre-processing

The multispectral images were pre-processed using Agisoft Metashape. The processing steps involved: (i) reflectance calibration using the drone's inbuilt sun sensor; (ii) imagery alignment using high accuracy, generic preselection, reference preselection (source), 40,000 as the key point limit, 4,000 as the tie point limit, and excluding stationary tie points; (iii) dense point cloud building, with medium quality and moderate filtering; (iv) Digital Elevation Model (DEM) building, using the point cloud as source data and enabling interpolation; (v) orthomosaic building, using the DEM as surface, "mosaic" as blending mode, and enabling hole filing. The resulting orthomosaic and DEM were exported as raster files. The orthomosaic was composed of a five-layered raster, each layer containing reflectance data from one of the multispectral bands: blue (450 ± 16 nm), green (560 ± 16 nm), red (650 ± 16 nm), red edge (RE; 730 ± 16 nm), and near infrared (NIR; 860 ± 26 nm). Green and red bands were duplicated in the exported raster, since they were derived from both the RGB and multispectral cameras, but the ones coming from the RGB camera were excluded from further analysis to avoid redundancy. Therefore, we used the blue band from the RGB camera and the green and red bands from the multispectral camera.

Thermal images were corrected and converted from JPEG to TIF files using the "theRmalUAV" R package (Metsu et al., 2025). Such conversion is needed since the Mavic M3T measures at-sensor temperature, while we were interested in land surface temperature (Metsu et al., 2025). Additionally, data are stored as digital numbers, not actual temperature values. The package requires in situ measurements of temperature and humidity, flight height (to correct for atmospheric interference), background temperature (estimated according to the sky condition during the flight, which can be skyclear or overcast, respectively "TRUE" or "FALSE" in the "SKC" argument), and surface emissivity. The latter was estimated using the package based on the Normalized Difference Vegetation Index (NDVI) data (more details in (Metsu et al., 2025)), which we derived from the multispectral images (Fig. 2). The package provides as output TIF files with actual land surface temperature values in centikelvin. The values were converted to Celsius by dividing them by 100 and subtracting 273.15. The images were pre-processed in Agisoft Metashape, following the same steps as described above for the multispectral imagery, with the only difference being that the result is a raster file with a single band containing temperature information. The alignment of the thermal and multispectral raster files was done in QGIS v3.28.12, using the "georeferencer" tool and ground control points located in the field site. The settings used in the tool were a linear transformation type and a cubic resampling method. All other settings were left as default. After corrections, the output was a land surface temperature (LST) orthomosaic with temperature values in C (Fig. 2).

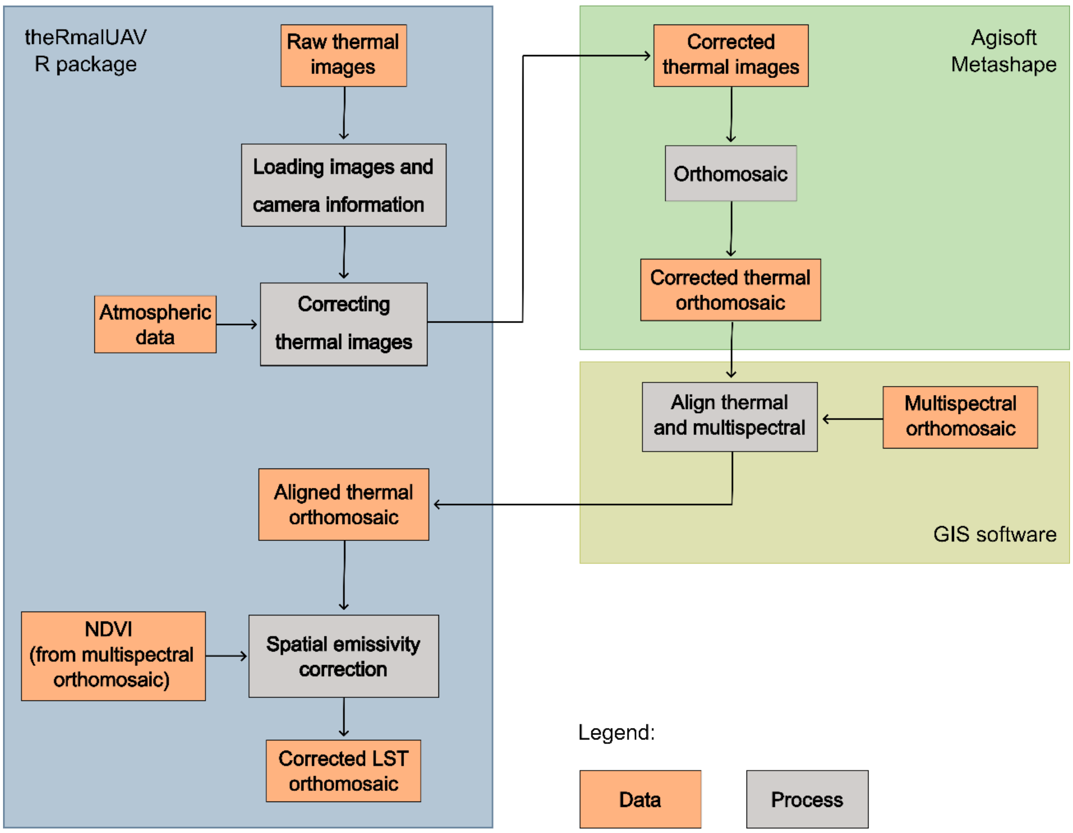

Fig. 2. Workflow for the processing of drone thermal imagery. The workflow uses the "theRmalUAV" R package (Metsu et al., 2025), Agisoft Metashape, and a GIS software. The output is an orthomosaic containing land surface temperature values in degrees Celsius.

With the multispectral and LST orthomosaic images, we derived predictor variables to train the RF model, including reflectance values from each multispectral band (blue, green, red, RE, and NIR), LST, NDVI (Tucker, 1979), Normalized Difference Water Index (NDWI; (McFeeters, 2013, 1996)), and texture layers derived from NDVI and LST data. Texture refers to the standard deviation of pixels within a moving window (e.g., (Lewis et al., 2022)), representing the local heterogeneity in vegetation (NDVI) and temperature (LST). We used moving windows of 5x5 and 7x7 pixels, resulting in two texture layers for each of these variables. The two distinct texture layers were used to represent more and less local heterogeneity.

2.4. Training and evaluating the Random Forest models

We trained RF models targeted to classify all pixels in the image as one of the three possible classes described in section 2.2. As reference data, we used vegetation type classes and as predictor variables, we used drone data. Since one of our goals was to investigate the impact of spatial resolution on the classification, we artificially generated rasters with distinct spatial resolutions ranging from 0.1 to 1.5 m. These resolutions were made by aggregating values of pixels in the fine-resolution images (originally with 1.3 cm for the multispectral and 3.8 cm for the thermal images) to coarser scales. We included resolutions of 0.1 m, 0.25 m, 0.5 m, 0.75 m, 1 m, 1.25 m, and 1.5 m.

Since finer spatial resolutions imply a higher number of available pixels for training the models, we under-sampled the training instances for finer spatial resolutions than 1.5 m, according to the number available for that coarsest resolution: 1620 for waterlogged and dry grasslands, and 419 for the "other" class. This selection guarantees that differences in the model's performance are due to differences in spatial resolution, not availability of training instances. Finally, since spatial autocorrelation can affect accuracy assessment (Roberts et al., 2017), we split the training and validation instances into spatial blocks, large enough so that spatial autocorrelation would have a low impact on the accuracy assessment. This step was done separately for each class. Within each class, 75% of the polygons were used for training and 25% for validation. This selection was done using the "blockCV" package in R (Hastie et al., 2009). Although such an approach might result in underestimated accuracies, it guarantees that the accuracy level achieved was due to the classification capabilities of the trained model, and not to validating the model with instances too close to the training instances (Roberts et al., 2017).

After splitting the training and validation datasets, we used the "caret" package in R (Kuhn, 2008) to train an RF model for each spatial resolution. We employed the "train" function and set the "method" to "rf", and "ntree" to 500. The "ntree" argument determines how many decision trees will be trained and combined (i.e., bagged) to form the final model. The remaining arguments were set as default. For each spatial resolution, we trained an RF model with and without including the thermal data, to assess the impact of the inclusion of this type of data on the grassland classification accuracy.

Once trained, each RF model was evaluated using the overall accuracy as the accuracy metric (Congalton, 1991). Since the "other" class had fewer validation instances than the grassland classes, we undersampled the number of validation instances from the waterlogged and dry grassland classes to match the number from the "other" class. Given that some instances might be easier to classify than others, potentially impacting the accuracy assessment, we iteratively repeated the validation process ten times with different random subsets and used the mean overall accuracy as the representative accuracy for that spatial resolution. This process guarantees that the achieved accuracy was not due to the subset of instances used.

To test for differences in the classification accuracies for distinct spatial resolutions (research question 1), we used a Kruskal-Wallis test followed by a Dunn's post-hoc test (KW). We also compared the accuracies of models with the same spatial resolution but with/without including the thermal data (research question 2). For this step, we applied a Mann-Whitney-U test (MWU) as only two groups were compared. Finally, using the best-performing model (i.e., best accuracy among the tested spatial resolutions and including or excluding thermal data), we derived predictor variable importance to identify which variables were fundamental for mapping different grassland types in the Cerrado (research question 3). We used the Gini importance metric to estimate the predictor variable importance (Hastie et al., 2009). We also used this model to generate a marginal effect plot for LST, to understand how distinct temperature levels influenced the classification decision made by the RF models.

Finally, the process was repeated for data sampled during the rainy season, to check for seasonal differences in the results.

2.5. Classification post-processing

To improve classification accuracy, two extra post-processing steps were taken. First, we used spatial interpolation to remove single pixels or isolated small patches of one grassland type surrounded by the other. Based on in situ knowledge, we knew that it was highly unlikely that small patches (i.e., < 5 m^2) of waterlogged grasslands occur in the middle of a dry grassland and vice versa. Therefore, these small patches were identified and their class was replaced by the grassland type surrounding them. Hereafter, we refer to this process as "patch size thresholding". Second, waterlogged grasslands were also predicted in high-elevation locations on the landscape, often close to trees. Waterlogged grasslands in these locations, far from the water table, were unlikely to occur. Moreover, high-elevation pixels with nearby trees classified as waterlogged grassland might represent an artefact of the model, which was classifying dry grasslands in shaded spots as waterlogged grasslands. To tackle this issue, we used the DEM derived from the drone imagery to set a threshold beyond which it was unlikely that waterlogged grasslands occurred. This step was done by extracting the elevation values from the DEM for all pixels classified as waterlogged grasslands and using the 95^{th} percentile to identify outliers (see Figure S1 in Supporting Information). These were converted to dry grasslands. The same process was performed for dry grasslands occurring in low elevations (i.e., close to the water table), using the 5^{th} percentile. Although using the 95^{th}

and 5^{th} percentiles was an arbitrary decision, these are common cutoff values for outlier removal in environmental sciences. Moreover, the thresholds made sense based on the field-sampled reference data: all reference points above the 95^{th} percentile were indeed dry grasslands (and the other way around for waterlogged grasslands). These two post-processing steps were not performed for the "other" class.

This post-processing resulted in what we called a "two-stage classification": in the first stage, the trained model predicted grassland types based on the provided drone data and in the second stage, we used ancillary data on elevation and a patch size thresholding to post-process the classification map as described above.

3. RESULTS

3.1. The impact of spatial resolution and thermal data on mapping accuracy

The best classification accuracies were achieved with intermediate spatial resolutions (between 0.75 and 1.25 m), both in the transition and wet seasons (Fig. 3a-b). No significant (KW: chi-squared = 66.2, $p < 0.05$, df = 6 for the transition season; chi-squared = 63.3, $p < 0.05$, df = 6 for the wet season) differences in overall accuracy were found among these three spatial resolutions, although 1.0 m had a slightly better average accuracy: 86.0% in the transition season and 90.2% in the wet season. These comparisons were made among the accuracies obtained using the thermal data. The same comparisons, but among the models without thermal data, can be found in Supporting Figure S2.

For all spatial resolutions tested, inclusion of the thermal data while training the RF model significantly improved (MWU: U = 0, $p < 0.05$, for all comparisons) the overall accuracy. In the transition season, the largest improvement was at a 0.75 m scale, with the overall accuracy increasing from 76.0% to 83.4%. The average improvement in this season, considering all spatial resolutions tested, was 4.2 percentage points. In the wet season, the largest improvement was at a 1.0 m scale, increasing from 81.2% to 90.2%. The average improvement was 7.3 percentage points.

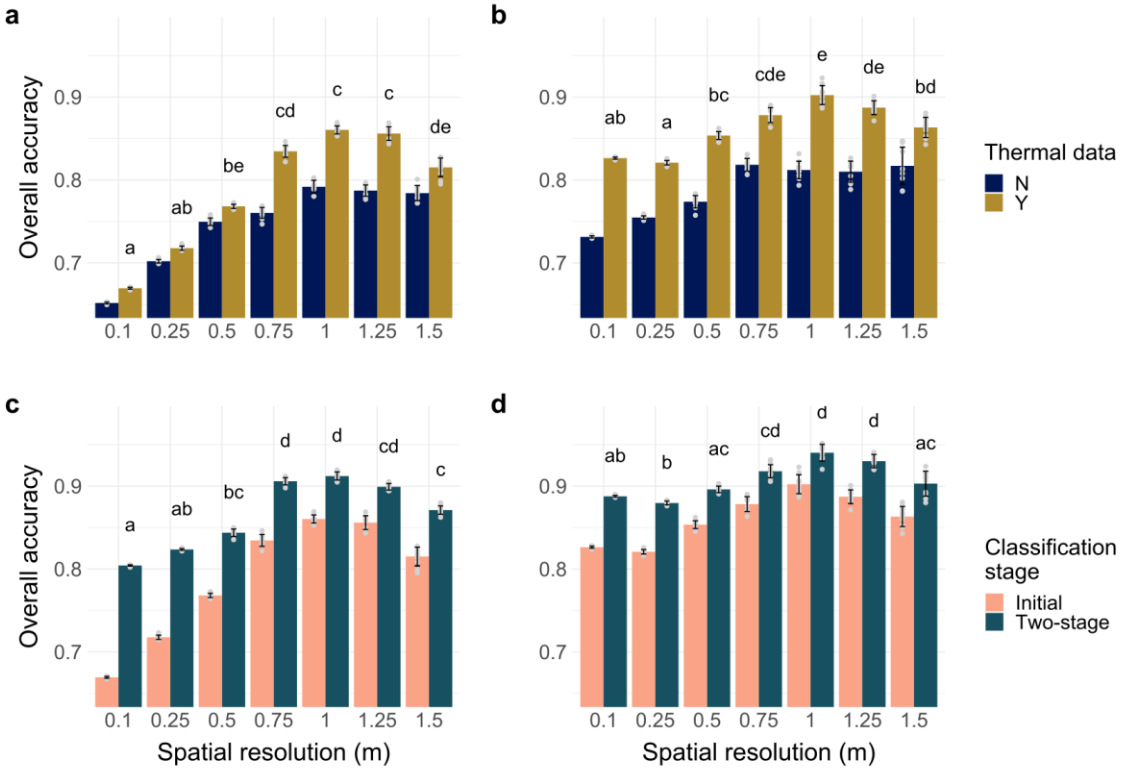

Fig. 3. Overall accuracy of the classification with distinct spatial resolutions and classification scenarios. Comparisons using thermal data (Y) or not (N) for the transition (a) and wet season (b) using the initial classification stage. Comparisons between the initial and two-stage classification in the transition (c) and wet season (d). The accuracy assessment was iteratively performed 10 times with a random subsample of the validation dataset (see section 2.3). The average value of the iterations is presented, with their respective error bars (± one standard deviation). The accuracy of each iteration is presented as gray points. Distinct letters represent significant differences in accuracy for distinct spatial resolutions (KW). Within resolution comparisons (i.e., differences between inclusion vs exclusion of thermal data, or between the initial vs two-stage classification, for a given resolution) are not shown in the plot, although in all cases the differences were significant (MWU).

3.2. Two-stage classification and variable importance

The additional post-processing steps (i.e., two-stage classification) significantly improved the overall accuracy of grassland classification across all spatial resolutions tested (MWU: U = 0, $p < 0.05$, for all comparisons). The patterns observed were the same as with initial classifications: increasing accuracy as spatial resolution decreased, up to 1.0 m, beyond which accuracy declined. Although the model trained with 1.0 m resolution presented a slightly better overall accuracy (91.2% in the transition and 94.0% in the wet season), no significant differences were found among the 0.75, 1.0, and 1.25 m scales, both in the transition and wet season (Fig. 3c-d). On average, in the transition season, the two-stage classification performed 7.7 percentage points better than the initial one. In the wet season, the average improvement was 4.6 percentage points. In the wet season, the difference in mapped wetland area between the initial and two-stage classification was of 0.79 ha (i.e., 26.19 and 25.4 ha, respectively; see classification maps for the wet season in Figure S3 in the Supporting Information).

Next, we tested differences in predictor variable importance. In the transition season, the most important variable to classify grassland types was NDVI, while in the wet season, LST was the most important (Fig. 4a-b). For both seasons, the likelihood of a pixel being classified as waterlogged grassland increased at low temperatures (~36 °C in the transition season and 34 °C in the wet season), while increasing temperatures (~39 °C in both seasons) were related to a greater likelihood of dry grassland classification (Figs. 4c-d, S4 Supporting Information).

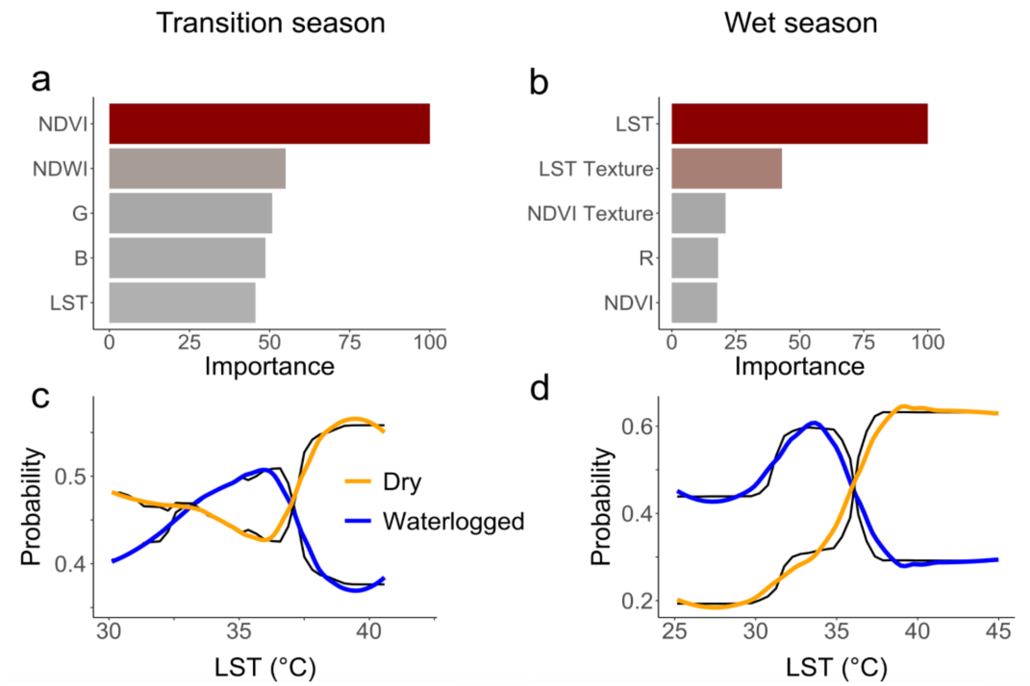

Fig. 4. Variable importance and marginal effect plots. Importance of the five most important predictor variables for the model trained in the transition (a) and wet (b) seasons, measured as the mean decrease in Gini impurity standardized to vary from 0 to 100. Marginal effect plots showing the probability of pixels being classified as either a waterlogged or dry grassland according solely to the LST data. Plots derived from the transition (c) and wet (d) season Random Forest models. Marginal effect plots for NDVI are shown in Figure S5 in Supporting Information.

4. DISCUSSION

Here, our multi-step workflow provided a significant advance in mapping accuracy of Cerrado wetlands. We accomplished these goals through determining the optimal spatial resolution and inclusion of thermal and topography data, as well as patch size thresholding. Our methods are robust and repeatable and the code is free and accessible. For endangered Cerrado wetlands, knowing where they occur is the first step toward protecting them. In the following sections, we highlight our main findings and the importance of application of these results.

4.1 Key factors affecting grassland classification

The spatial resolution of drone imagery used to classify the study site into either waterlogged or dry grassland had a significant impact on mapping accuracy. Changes in overall accuracy showed a clear pattern: a gradual increase in accuracy from fine to coarse resolutions, up to 1.0 m, after which accuracy declined. Studies in agricultural fields and forests found similar results, with specific resolutions providing optimal results (Liu et al., 2020; Meddens et al., 2011). Here, we found that the optimal spatial resolution for mapping Cerrado wetlands was between 0.75 and 1.25 m, with no significant differences in performance among these resolutions, although 1.0 m showed a slightly better overall accuracy. This result is probably because 1.0 m is closer to the grain size of the object being classified, i.e., a plant community (Jensen, 2007). Resolutions that are too fine (e.g., 10 and 25 cm) add confusion to the trained algorithm, compromising an accurate classification, while too coarse resolutions (e.g., 1.5 m) do not provide the necessary level of detail for accurately mapping the different grassland types (Meddens et al., 2011; Woodcock and Strahler, 1987).

Another factor that significantly affected mapping accuracy was the inclusion of thermal data for training the RF algorithm. For all spatial resolutions tested, inclusion of thermal data significantly improved overall accuracy, providing answers about the utility of thermal data as a complement to multispectral. On average, the models that included thermal data performed 4.2 percentage points better in the transition season and 7.3 percentage points better in the wet season. Achieving higher accuracies when using thermal data highlights the importance of using LST information to better distinguish waterlogged from dry grasslands in multi-time point Cerrado land cover mapping. While LST in dry grasslands is highly variable throughout the year, the high soil water availability in permanently and seasonally waterlogged grasslands results in higher evapotranspiration rates, leading to increased evaporative and transpiration cooling and lower temperatures locally (Fleischmann et al., 2023; Rodrigues et al., 2014; Wu et al., 2021). LST is also lower in waterlogged soils, even during warmer seasons, since the higher heat capacity of these soils makes them warm up slower than their dry counterparts (Gan et al., 2012; Hillel, 2003).

Lastly, by using data on landscape topography and applying a patch size threshold to the classification maps generated (i.e., two-stage classification), we significantly improved mapping accuracy. In both seasons, the two-stage classification performed significantly better than the initial one: on average, 7.7 percentage points in the transition and 4.6 in the wet season. Although a 4.6 percentage point improvement might not sound substantial, it is important to remember that the overall accuracy went from 81.2% (initial classification without thermal data) to 94.0% (using thermal data and the two-stage classification) in the wet season.

Besides the high accuracy obtained, we improved wetland extent estimation for the study area. While current state-of-the-art land cover maps showed a 5.6 ha wetland area overlapping with our study site (MapBiomas, 2024a), our maps for the wet season, i.e., when wetlands reach their largest extent, showed an area of 25.4 ha, a 4.5x increase (see Figure S6 in Supporting Information). This large mismatch is most probably due to methodological decisions, as we will discuss further below (section 4.3).

4.2 Temperature and vegetation greenness are important predictors for grassland classification

Among the predictor variables used, LST and NDVI appeared among the top five most important both in the transition (5^{th} and 1^{st}, respectively) and wet (1^{st} and 5^{th}, respectively) seasons. Including thermal data for RF model training was especially important in the wet season (see above, section 4.1). In the transition season, since some rainfall had already fallen in the ecosystems, grassy vegetation in parts of the dry grasslands were starting to green up. This partial transition resulted in considerable variation in vegetation greenness within dry grasslands in this season. Meanwhile, in the wet season, when soil water is widely available for both grassland types, vegetation in both should be green, making it harder to distinguish solely based on greenness. This variation in greenness due to distinct rainfall availability in each season helps explain why NDVI shifted from the most important variable in the transition season to the 5th in the wet season. This pattern was also observed in the marginal effect plots of NDVI: while the transition season plot had larger probability differences for low and high NDVI values, the wet season plot had similar probabilities across the range of NDVI values.

These results align with findings by Nemani and Running (Nemani and Running, 1997), who mapped land cover types in North America using satellite data and found similar NDVI values between irrigated crops and broadleaf forests, while their temperature profiles differed. Moreover, these results strengthen our argument regarding the importance of using thermal data for differentiating vegetation types, mainly in the wet season, aligning with studies conducted in other regions with spaceborne remote sensing data (Eisavi et al., 2015; Sun and Schulz, 2015).

4.3 An urgent need to better protect Cerrado wetlands

The Cerrado is a cornerstone of South American hydrology, harboring the headwaters of approximately two-thirds of Brazil’s major watersheds (Durigan et al., 2022; Lima and Silva, 2007). Cerrado wetlands, including permanently and seasonally waterlogged grasslands, buffer excess rainfall and slowly release water throughout the year, sustaining perennial rivers and securing water provision far beyond the biome's boundaries (Bassani et al., 2025; Durigan et al., 2022).

Legally, springs and concentrated seeps receive formal protection, but equivalent safeguards were not historically applied to diffuse seep-formed wetlands such as waterlogged grasslands occurring in interfluves (Bassani et al., 2025). Recent legal interpretation argues that Brazil's existing environmental framework already enables the recognition of non-floodplain wetlands as seep-formed ecosystems, supporting stronger protection for waterlogged grasslands (Bassani et al., 2025). Despite this, current national-scale land cover maps detect only permanently flooded wetlands in the Cerrado, due to the use of dry-season data for their classifications (MapBiomas, 2024b, 2024a). This dry-season focus leads to a systematic underestimation of wetland extent. Although such an underestimation is understandable due to methodological decisions, we stress here the importance of both estimating wetland area extent in different seasons and targeting mapping of seep-formed wetlands, which account for the majority of Cerrado wetlands (Bassani et al., 2025). Both are important steps for a more accurate carbon accounting and precise estimates of water-related ecosystem services provision by Cerrado landscapes.

Given accelerating agricultural expansion in the Cerrado (Ribeiro et al., 2011), accurately mapping Cerrado waterlogged grasslands across seasons is essential to enforce legal protection, and therefore, preserve downstream ecosystem services. Our findings, by showing improved accuracies with spatial resolutions close to 1 m and thermal data fusion across space and time, helped address this need by advancing wetland detectability at ecologically relevant scales.

4.4 Conclusions

In this study, we found that both the spatial scale and use of thermal data had a significant impact on accuracy of Cerrado grassland mapping. By comparing our drone-based wetland maps with state-of-the-art satellite-derived land cover maps for Brazil, we identified a wetland extent more than four times larger in our study area than previously reported, illustrating how the occurrence of these ecosystems is often underestimated. With these findings, we advocate for an increased focus on a more accurate mapping of Cerrado wetlands (and seasonal wetlands more broadly). These ecosystems have patchy vegetation types that are challenging to map yet represent major carbon and water stores, serving as the headwaters of Brazil's most important rivers. From a management perspective, accurately mapping waterlogged grasslands and their boundaries with dry grasslands provides essential information for the delineation of areas to be legally protected and managed (e.g., for biodiversity, carbon storage or fire). For example, given the seasonal nature of many of the Cerrado wetlands, fire is a natural and necessary process in these ecosystems; this is a very different situation to other Brazilian permanent wetlands, e.g., the Amazon or Pantanal, although with climate change even these systems are at increasing risk of droughts and fire. Importantly, optimal fire regimes differ among ecosystems and even grassland types. By accurately mapping these different grassland types across seasons, we can identify where seasonal wetlands occur. The delineation of seasonal wetlands is important since they behave differently from ever-wet or ever-dry grasslands, e.g., in terms of gas emissions and plant productivity in different seasons (Verona et al., 2026). With greater knowledge of how they function and how large they are, we can more accurately estimate their shifting contributions to water and carbon dynamics across seasons. Ultimately, our workflow and findings provide novel tools for a more accurate future upscaling of Cerrado wetland mapping, e.g., to state, biome, and even country levels, enabling improved assessment of their role in carbon storage and fluxes.

DATA AVAILABILITY

The drone multispectral and thermal images used in this study, together with the classification of the study area in the transition and wet seasons are made available at https://doi.org/10.5281/zenodo.18304662.

ACKNOWLEDGEMENTS

This work was supported, in part, by an NSF award (DEB-2507959) to AEZ, in part by a FWO-FAPESP bilateral collaboration award (reference number G0F6922N and 2021/05592-0, respectively) to BS and RSO. CM was funded by Internal Funds of KU Leuven (MICROMICS project; C14/22/067). We would like to thank Ved Chirayath for the drone flight and data processing training; Genevive Noyce and Roy Rich for field project sampling suggestions; Alessandra Bassani and Thales Scarpato for assistance during field campaigns; and Maria Carolina Alves de Camargo and other staff from the Chapada dos Veadeiros National Park for the administrative support during field campaigns. The authors declare that there is no conflict of interest regarding the publication of this article.

REFERENCES

Adam, E., Mutanga, O., Rugege, D., 2010. Multispectral and hyperspectral remote sensing for identification and mapping of wetland vegetation: A review. Wetl. Ecol. Manag. 18, 281–296. https://doi.org/10.1007/s11273-009-9169-z

Bassani, A., Pilon, N.A.L., Peixoto, F.P., Mattos, C.R.C., Silveira, F.A.O., Cunha, L.S. da, Oliveira, R.S., 2025. Legally protected, practically overlooked: The neglect of diffuse seeps in the conservation of Cerrado non-floodplain wetlands. Perspect. Ecol. Conserv. 23, 151–156. https://doi.org/10.1016/j.pecon.2025.06.001

Congalton, R.G., 1991. A review of assessing the accuracy of classifications of remotely sensed data. Remote Sens. Environ. 37, 35–46.

Durigan, G., Munhoz, C.B., Zakia, M.J.B., Oliveira, R.S., Pilon, N.A.L., Valle, R.S.T. do, Walter, B.M.T., Honda, E.A., Pott, A., 2022. Cerrado wetlands: multiple ecosystems deserving legal protection as a unique and irreplaceable treasure. Perspect. Ecol. Conserv. https://doi.org/10.1016/j.pecon.2022.06.002

Eisavi, V., Homayouni, S., Yazdi, A.M., Alimohammadi, A., 2015. Land cover mapping based on random forest classification of multitemporal spectral and thermal images. Environ. Monit. Assess. 187, 1–14. https://doi.org/10.1007/s10661-015-4489-3

Fleischmann, A.S., Laipelt, L., Papa, F., Paiva, R.C.D. de, de Andrade, B.C., Collischonn, W., Biudes, M.S., Kayser, R., Prigent, C., Cosio, E., Machado, N.G., Ruhoff, A., 2023. Patterns and drivers of evapotranspiration in South American wetlands. Nat. Commun. 14. https://doi.org/10.1038/s41467-023-42467-0

Funk, C., Peterson, P., Landsfeld, M., Pedreros, D., Verdin, J., Shukla, S., Husak, G., Rowland, J., Harrison, L., Hoell, A., Michaelsen, J., 2015. The climate hazards infrared precipitation with stations - A new environmental record for monitoring extremes. Sci. Data 2, 1–21. https://doi.org/10.1038/sdata.2015.66

Gan, L., Peng, X., Peth, S., Horn, R., 2012. Effects of grazing intensity on soil thermal properties and heat flux under Leymus chinensis and Stipa grandis vegetation in Inner Mongolia, China. Soil Tillage Res. 118, 147–158. https://doi.org/10.1016/j.still.2011.11.005

Google Earth, 7.3.2.5491, 2018. Chapada dos Veadeiros, Brazil, lat -14.186 °, lon -47.569 °. Imag. ©2023 CNES/Airbus Maxar Technol. Retrieved March 23, 2023 from https//www.google.com/earth/index.html.

Hastie, T., Tibshirani, R., Friedman, J., 2009. The Elements of Statistical Learning - Data Mining, Inference, and Prediction, 2nd ed. Springer, New York, USA.

Hemes, K.S., Eichelmann, E., Chamberlain, S.D., Knox, S.H., Oikawa, P.Y., Sturtevant, C., Verfaillie, J., Szutu, D., Baldocchi, D.D., 2018. A Unique Combination of Aerodynamic and Surface Properties Contribute to Surface Cooling in Restored Wetlands of the Sacramento-San Joaquin Delta, California. J. Geophys. Res. Biogeosciences 123, 2072–2090. https://doi.org/10.1029/2018JG004494

Hillel, D., 2003. Introduction to environmental soil physics. Elsevier, San Diego, USA.

Jarocińska, A., Kopeć, D., Niedzielko, J., Wylazłowska, J., Halladin-Dąbrowska, A., Charyton, J., Piernik, A., Kamiński, D., 2023. The utility of airborne hyperspectral and satellite multispectral images in identifying Natura 2000 non-forest habitats for conservation purposes. Sci. Rep. 13, 1–16. https://doi.org/10.1038/s41598-023-31705-6

Jensen, J.R., 2007. Remote Sensing of the Environment: An Earth Resource Perspective. Prentice Hall, Upper Saddle River, NJ, USA.

Kuhn, M., 2008. Building predictive models in R using the caret package. J. Stat. Softw. 28, 1–26.

Lewis, K., Barros, F. de V., Cure, M.B., Davies, C.A., Furtado, M.N., Hill, T.C., Hirota, M., Martins, D.L., Mazzochini, G.G., Mitchard, E.T.A., Munhoz, C.B.R., Oliveira, R.S., Sampaio, A.B., Saraiva, N.A., Schmidt, I.B., Rowland, L., 2022. Mapping native and non-native vegetation in the Brazilian Cerrado using freely available satellite products. Sci. Rep. 12. https://doi.org/10.1038/s41598-022-05332-6

Lima, J.E.F.W., Silva, E.M., 2007. Estimativa da contribuição hídrica superficial do Cerrado para as grandes regiões hidrográficas brasileiras, in: XVII Simpósio Brasileiro de Recursos Hídricos. p. 13.

Liu, M., Yu, T., Gu, X., Sun, Z., Yang, J., Zhang, Z., Mi, X., Cao, W., Li, J., 2020. The Impact of Spatial Resolution on the Classification of Vegetation Types in Highly Fragmented Planting Areas Based on Unmanned Aerial Vehicle Hyperspectral Images. Remote Sens. 12, 1–25.

Maes, W.H., 2025. Practical Guidelines for Performing UAV Mapping Flights with Snapshot Sensors. Remote Sens. 17, 1–38.

MapBiomas, 2024a. MapBiomas General “Handbook”: Algorithm Theoretical Basis Document (ATBD) - Collection 9 Version 2.

MapBiomas, 2024b. MapBiomas: Cerrado - Appendix - Collection 9 Version 1.

McFeeters, S.K., 2013. Using the normalized difference water index (ndwi) within a geographic information system to detect swimming pools for mosquito abatement: A practical approach. Remote Sens. 5, 3544–3561. https://doi.org/10.3390/rs5073544

McFeeters, S.K., 1996. The use of the Normalized Difference Water Index (NDWI) in the delineation of open water features. Int. J. Remote Sens. 17, 1425–1432. https://doi.org/10.1080/01431169608948714

Meddens, A.J.H., Hicke, J.A., Vierling, L.A., 2011. Evaluating the potential of multispectral imagery to map multiple stages of tree mortality. Remote Sens. Environ. 115, 1632–1642. https://doi.org/10.1016/j.rse.2011.02.018

Metsu, C., Maes, W.H., Ottoy, S., Van Meerbeek, K., 2025. theRmalUAV : An R package to clean and correct thermal UAV data for accurate land surface temperatures. Methods Ecol. Evol. 00, 1–9. https://doi.org/10.1111/2041-210x.70196

Muro, J., Strauch, A., Heinemann, S., Steinbach, S., Thonfeld, F., Waske, B., Diekkrüger, B., 2018. Land surface temperature trends as indicator of land use changes in wetlands. Int. J. Appl. earth Obs. Geoinf. 70, 62–71.

Myers, N., Mittermeier, R.A., Mittermeier, C.G., Fonseca, G.A.B., Kent, J., 2000. Biodiversity hotspots for conservation priorities. Nature 403, 853–858. https://doi.org/10.1080/21564574.1998.9650003

Nemani, R., Running, S., 1997. Land cover characterization using multitemporal red, near-IR, and thermal-IR data from NOAA/AVHRR. Ecol. Appl. 7, 79–90. https://doi.org/10.1890/1051-0761(1997)007[0079:LCCUMR]2.0.CO;2

Oke, T.R., 1987. Boundary layer climates. Routledge, London, United Kingdom.

Ribeiro, J.F., Walter, B.M.T., 2008. As principais fitofisionomias do bioma Cerrado. Cerrado Ecol. e flora 1, 151–212.

Ribeiro, S.C., Fehrmann, L., Soares, C.P.B., Jacovine, L.A.G., Kleinn, C., de Oliveira Gaspar, R., 2011. Above- and belowground biomass in a Brazilian Cerrado. For. Ecol. Manage. 262, 491–499. https://doi.org/10.1016/j.foreco.2011.04.017

Roberts, D.R., Bahn, V., Ciuti, S., Boyce, M.S., Elith, J., Guillera-Arroita, G., Hauenstein, S., Lahoz-Monfort, J.J., Schröder, B., Thuiller, W., Warton, D.I., Wintle, B.A., Hartig, F., Dormann, C.F., 2017. Cross-validation strategies for data with temporal, spatial, hierarchical, or phylogenetic structure. Ecography (Cop.).

40, 913–929. https://doi.org/10.1111/ecog.02881
Rodrigues, T.R., Vourlitis, G.L., Lobo, F.D.A., De Oliveira, R.G., Nogueira, J.D.S., 2014. Seasonal variation in energy balance and canopy conductance for a tropical savanna ecosystem of south central Mato Grosso, Brazil. J. Geophys. Res. Biogeosciences 119, 1–13. https://doi.org/10.1002/2013JG002472
Sawyer, D., 2009. Fluxos de carbono na Amazônia e no Cerrado: um olhar socioecossistêmico. Soc. e Estado 24, 149–171. https://doi.org/10.1590/s0102-69922009000100007
Steenvoorden, J., Limpens, J., 2023. Upscaling peatland mapping with drone-derived imagery: impact of spatial resolution and vegetation characteristics. GIScience Remote Sens. 60. https://doi.org/10.1080/15481603.2023.2267851
Sun, L., Schulz, K., 2015. The improvement of land cover classification by thermal remote sensing. Remote Sens. 7, 8368–8390. https://doi.org/10.3390/rs70708368
Tucker, C.J., 1979. Red and photographic infrared linear combinations for monitoring vegetation. Remote Sens. Environ. 8, 127–150.
Verona, L., Zanne, A., Trumbore, S., Bernardino, P.N., Alencar, G., Andreuccetti, T., Herrera Ramirez, D., Cardoso, J.C., Martins, D., Mazzochini, G., Pilon, N., Oliveira, R., 2026. Vast, overlooked peat and organic soils in Brazil's Cerrado: carbon storage, dynamics, and stability. New Phytol.
Woodcock, C.E., Strahler, A.H., 1987. The Factor of Scale in Remote Sensing. Remote Sens. Environ. 21, 311–332.
Wu, Y., Xi, Y., Feng, M., Peng, S., 2021. Wetlands cool land surface temperature in tropical regions but warm in boreal regions. Remote Sens. 13. https://doi.org/10.3390/rs13081439

SUPPORTING INFORMATION

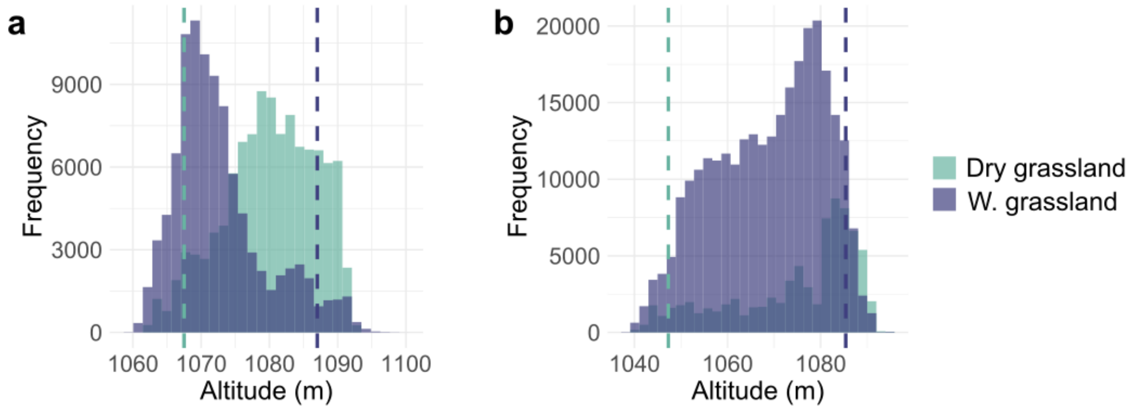

Figure S1. Elevation where distinct grassland types occur and identification of outliers. The 5th and 95th percentiles (dashed lines) were used, respectively, to identify lower outliers for dry grasslands and upper outliers for waterlogged grasslands ("w. grassland" in the legend). The plots represent the outlier identification in the transition (a) and wet (b) season.

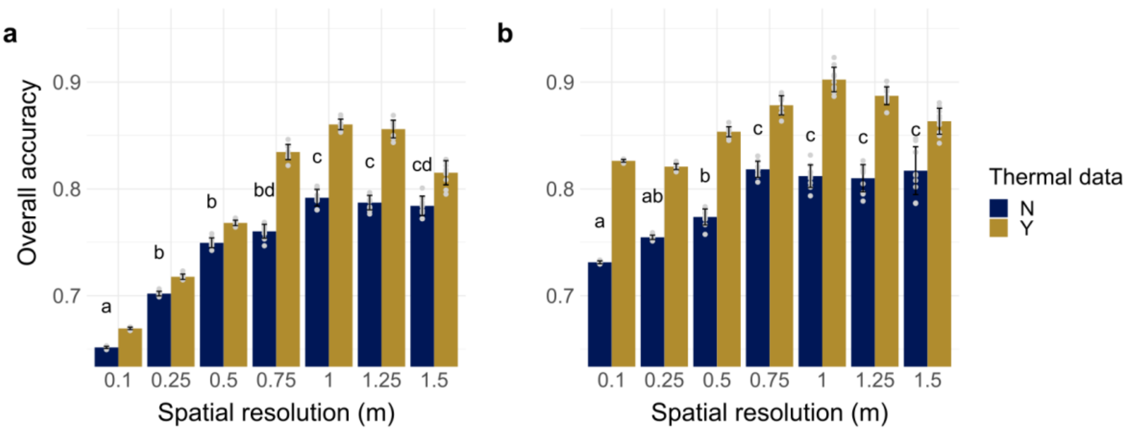

Figure S2. Overall accuracy of the classification with distinct spatial resolutions and for different classification scenarios. Comparisons using thermal data (Y) or not (N) for the transition (a) and wet season (b) using the initial classification stage. The accuracy assessment was iteratively performed 10 times with a random subsample of the validation dataset (see section 2.3 in the main text). The average value of the iterations is presented, with their respective error bars (± one standard deviation). The accuracy of each iteration is presented as gray points. Distinct letters represent significant differences in accuracy for distinct spatial resolutions, comparing the models trained without thermal data, according to a Kruskal-Wallis followed by a Dunn's test. Comparisons for the model with thermal data are presented in the main text (Fig. 3).

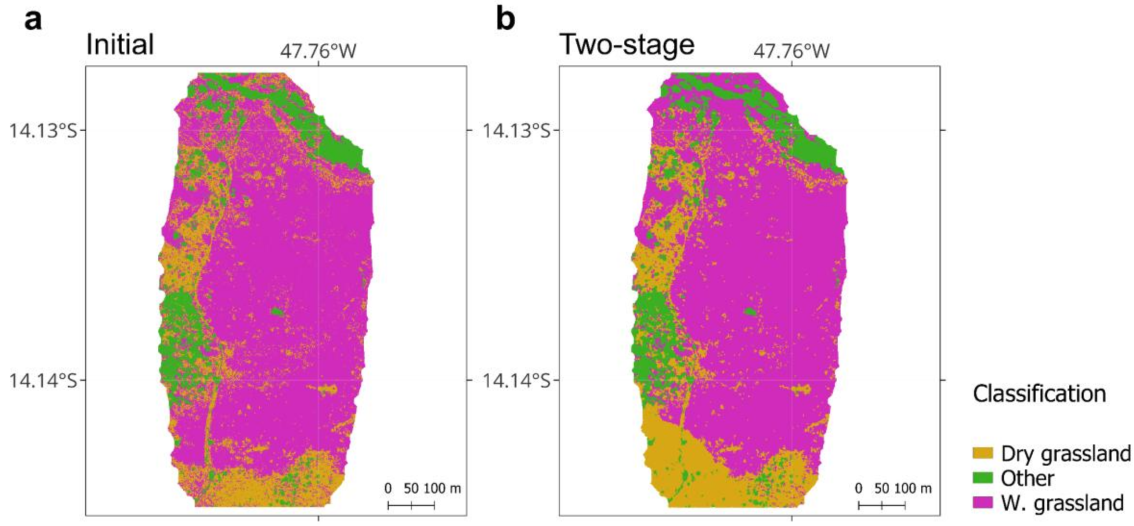

Figure S3. Classification map of the study site in the wet season. The maps were made using the initial (a) and two-stage (b) classification approaches. W. grassland: waterlogged grassland.

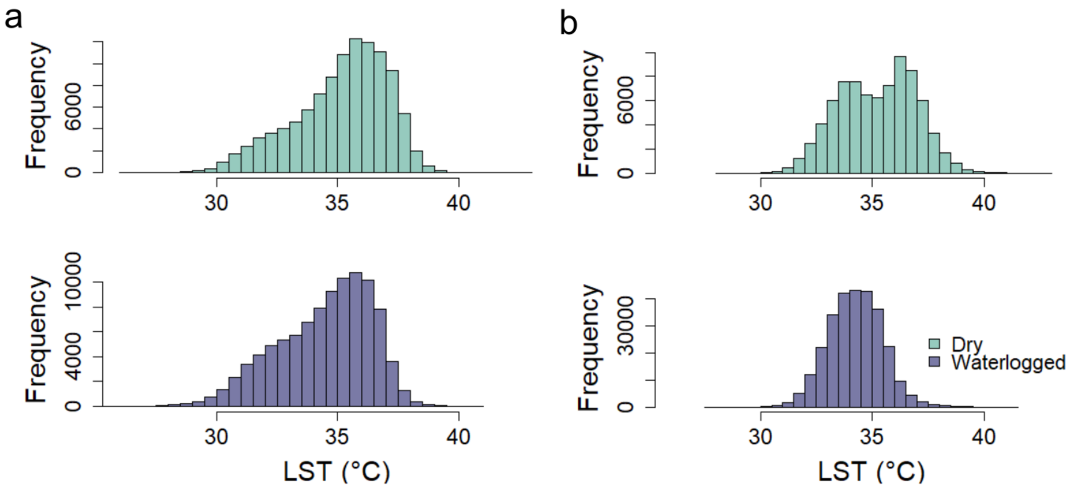

Figure S4. Distribution of Land Surface Temperature (LST) values for the two grassland types mapped. The values are presented for the transition season (a) and for the wet season (b). Note that the y-axes show a different range of values, since using the same range would hamper the visualization of dry grasslands distribution, mainly in the wet season, when their area is very limited.

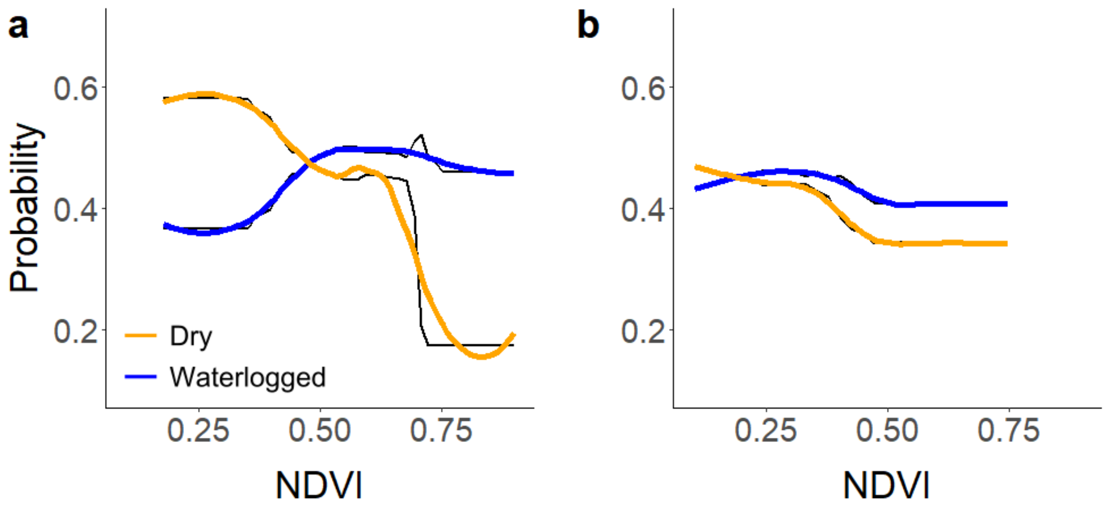

Figure S5. Marginal effect plots for the NDVI predictor variable. The plots show the probability of pixels being classified as either a waterlogged or dry grassland according solely to the NDVI data. Plots derived from the transition season (a) and wet season (b) RF models.

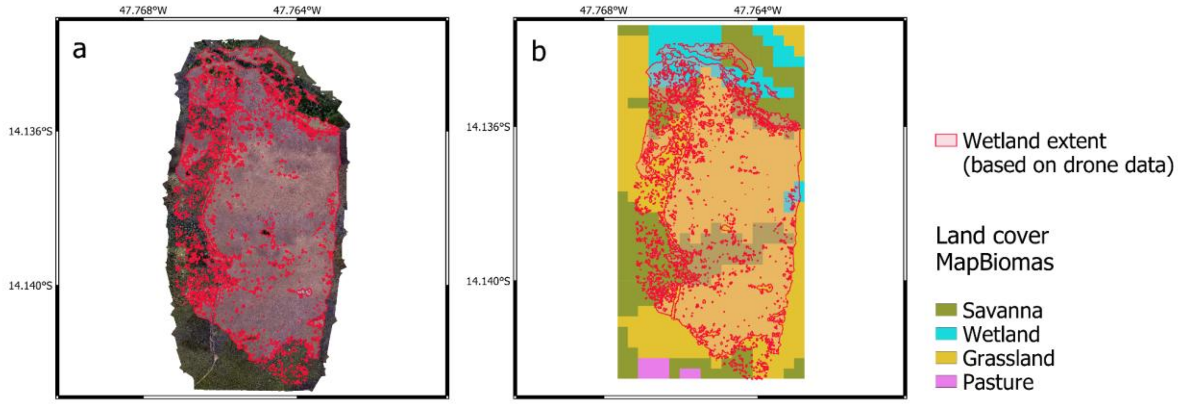

Figure S6. Mapped wetland extent using drone and satellite data. The rainy season wetland area mapped in this study (a), using multispectral and thermal drones, was 25.4 ha. MapBiomas Collection 9 land cover map (MapBiomas, 2024a), which uses dry season satellite data at 30 m spatial resolution, mapped only 5.6 ha in the overlapping area in 2022 (b).